physica status solidi pss a
www.pss-a.com

Check for updates

# The Structural, Optical, and Electrical Characterization of Ti/n-InP Schottky Diodes with Graphene Oxide Interlayer Deposited by Spray Pyrolysis Method

*Fulya Esra Cimilli Çatır*

**Ti/GO/n-InP Schottky barrier diode (SBD) is obtained by growing graphene oxide (GO) film on n/InP semiconductor using easy and economical spray pyrolysis method. The effect of GO as the interfacial layer on device performance of Ti/GO/n-InP SBD is investigated in detail. The optical absorbance spectra show that bandgap energy of the GO film is 3.57 eV. The optical transmittance value of 79.5% is in consistent with the absorbance spectra of GO film. The barrier heights (BHs) that are estimated for the Ti/GO/n-InP SBD vary from 0.263 to 0.980 eV (*I–V*) and 1.328 to 1.006 eV (*C–V*) from the *I–V* and *C–V* measurements in the temperature range of 100–400 K. The contradiction between the BHs from the *I–V* and *C–V* characteristics is discussed. The mean BH values are found to be $\Phi_{b01} = 0.98$ eV (250–400 K) and $\Phi_{b02} = 0.73$ eV (100–250 K) from the $\Phi_{b0}$–$1/2kT$ plot. From the modified Richardson plots based on a Gaussian distribution of BH, $\Phi_{b01} = 0.93$ (250–400 K) and $\Phi_{b02} = 0.69$ eV (100–250 K) and $A^*$ is calculated to be 12.44 and 12.73 A cm$^{-2}$ K$^{-2}$, respectively. The *I–V–T* and *C–V–T* measurements demonstrate that carrier transport mechanism of Ti/GO/n-InP is well explained by thermionic emission (TE) mechanism with a double Gaussian distribution of the Schottky barrier heights (SBHs).**

## 1. Introduction

Recently, among the carbon nanomaterials, graphene and graphene oxide (GO) have received significant attention by researchers. Although graphene has extraordinary electrical, optical, mechanical, and thermal properties, the use of graphene is limited by the lack of an electronic bandgap.[1] As a result, many researchers have concentrated their work on grapheme-based materials such as GO with tunable electronic properties. Unlike graphene, GO containing hydrogen and oxygen in its structure has been obtained by Brodie, Staundenmaier, Offeman, and Hummers methods since the early 19th century.[2] Modified Hummers method is widely used to obtain GO from graphite.[3] When compared with the other methods, less chemical toxicity and toxic gas are produced in the modified Hummers method. It is an easy and inexpensive method for producing higher amounts of GO.[4] The degree of oxidation in GO varies according to the method used, reaction conditions, and the properties of graphite.[4,5]

The GO is oxidized by strong oxidants, so the basic structure of GO is known as covalently bonded oxygen functional groups, epoxy or hydroxide group, in particular carbonyl and carboxyl group. Having these functional groups makes it suitable for many important applications such as sensors, field-effect transistors (FETs), biomedical applications, polymer composites, energy-related materials, and paper-like materials. Due to its oxygenated nature, GO primarily acts as an insulator material, but the bandgap can be changed with the change in its elemental structure. Because GO is easily dispersed in solvents, its dielectric property, transparency, adjustable electronic properties and superior mechanical properties, and application areas of the GO are expanding day by day.[2]

GO has controllable bandgap, high transmittance, and controllable conductivity, so it has been used by some researchers as an interface layer in metal–semiconductor (MS) heterojunctions.[6] Phan et al. investigated the electrical parameters of the Al/GO/n-Si/Al contact by GO interlayer. They have evaluated junction parameters from the current–voltage (*I–V*) measurements of the contact under dark and different light intensities.[7] Liu et al. produced Au/GO/n-Si solar cells and used GO thin layer as an insulator between the metal and semiconductor. They reported higher power conversion efficiency for silicon solar cell and their results presented that the ability to create a low cost and solution processable insulation layer is suitable for wide application in photovoltaic and other optoelectronic devices.[8]

Indium phosphide is a III–V compound semiconductor with a direct bandgap at about 1.42 eV which is an attractive material with a wide range of technological uses in optoelectronics such as solar cells, photo detectors, and laser diodes.[9,10] MS contacts have been frequently used in integrated circuits and InP semiconductor is an important alternative to Si for producing MS contacts. However, a complete description of the current transport mechanism of a MS contact is still a challenging problem.

Son et al.[11] explained the deviation from the Richardson curves at low temperatures by means of the Tunneling current

Dr. F. E. Cimilli Çatır
Department of Electronic Technologies
Vocational School
Erzincan Binali Yildirim University
Erzincan 24200, Turkey
E-mail: fcatir@erzincan.edu.tr

The ORCID identification number(s) for the author(s) of this article can be found under https://doi.org/10.1002/pssa.202000125.

**DOI: 10.1002/pssa.202000125**

 © 2020 Wiley-VCH GmbH

mechanism. As mentioned in this and similar studies, many current mechanisms are recommended for Schottky barrier diodes (SBDs) with or without interface layer in the literature. Despite all of these, we do not have enough information about the current mechanisms of Schottky diodes. In his study with GO/n-InP, Gullu et al.[12] stated that the Schottky barrier can be improved due to the GO interface layer, and thus the electronic properties of the diode can be significantly changed. When considering these and similar studies, it is not enough to study only at room temperature both about current mechanisms of interfaced Schottky diodes and barrier height (BH) and its structure. As Cimilli et al.[13] and Kudryk et al.[14] stated, more realistic results can be obtained by examining the diode characteristics in a wide temperature range and using different methods to understand the structure of the BH and the effect of the interface layer on the current transmission mechanisms. In addition, it is well known that thin interface layers can significantly change the electrical characteristics of the MS contact.[15] Therefore, in this study, we aimed to investigate *I–V* and *C–V* characteristics of the prepared Ti/n-InP Schottky diodes with organic GO interlayer in wide temperature range to determine the dominant conduction mechanism of the diode and investigate the effect of GO interlayer on diode parameters. Therefore, Ti/GO/n-InP SBD was produced by producing GO film with cheap and simple spray pyrolysis method. The structure of GO film was analyzed in detail with scanning electron microscopy (SEM), X-ray diffraction (XRD), energy-dispersive X-ray spectroscopy (EDX), absorbance and transmittance spectra, and the effects of GO film on the electrical and optical properties of Ti/GO/n-InP diode. Current transmission mechanisms of this structure were evaluated in detail over a wide temperature range (100–400 K) with *I–V–T* and *C–V–T* methods and its usage in the technology was investigated. In our current work, titanium (Ti) metal is used as a Schottky contact layer because of its improved adhesion to the semiconductor and its low work function closed to n-InP that can provide the lowest forward voltage drop. The GO interlayer in-between Ti Schottky layer and InP semiconductor is used for increasing the BH so as to decrease the interface state density as indicated at previous works.[16–18]

## 2. Results and Discussion

As shown in **Figure 1**, the film exhibits very good adhesion to the semiconductor substrate surface and covers the semiconductor surface completely. The GO structure overlaps in layers in accordance with the literature.

In addition, the amount of carbon, oxygen, and other elements was determined by the EDX device integrated into the SEM system. The carbon (C) and the oxygen (O) ratio in the GO was found to be 44.25 and 15.78, respectively, and the carbon/oxygen ratio was 2.80 in consistent with the literature.[4,19]

**Figure 2** shows that the XRD patterns of GO exhibited a peak at $2\theta = 10.1^\circ$ with an interlayer distance of 0.85 nm. As seen in the XRD spectra, the GO film was deposited successfully according to the literature.[20] Absorption and transmittance characteristics of GO film are shown in **Figure 3**a,b. When the absorbance spectrum is examined, it is noteworthy that the film acts as an opaque material due to its high absorption properties at short wavelengths. The absorbance values of the film increase sharply due to the increase in absorption characteristics of the films at wavelengths shorter than about 300 nm. This region, where a sharp increase in absorbance values is observed, is the main absorption region of the film. To determine the optical bandgap of GO film, Tauc's model was used and the plot of $(Ah\nu)^2$ versus the photon energy $h\nu$ and the absorption bandgap ($E_g$) can be determined by the equation: $(Ah\nu)^2 = a(h\nu - Eg)$,[21] where $h\nu$ is the photon energy (eV), $A$ is the absorption coefficient, $a$ is a constant, and $Eg$ is the bandgap. The $(Ah\nu)^2$ versus $h\nu$ plot of GO film is shown in Figure 3a. The optical bandgap energy of the GO film can be determined from extrapolation of linear region of the plot at $(Ah\nu)^2 = 0$. From the absorbance spectra, it was determined that the film was a material with a direct

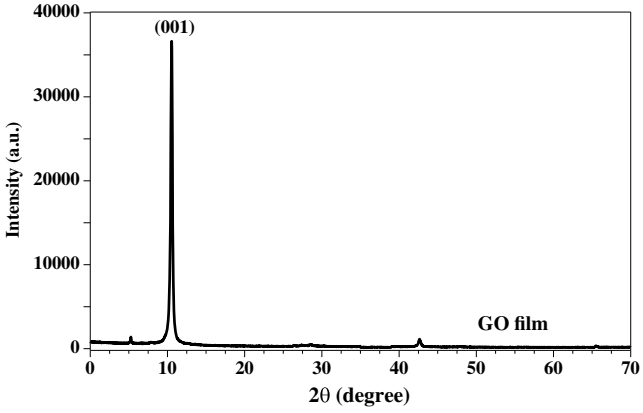



**Figure 2.** XRD spectra of GO film.

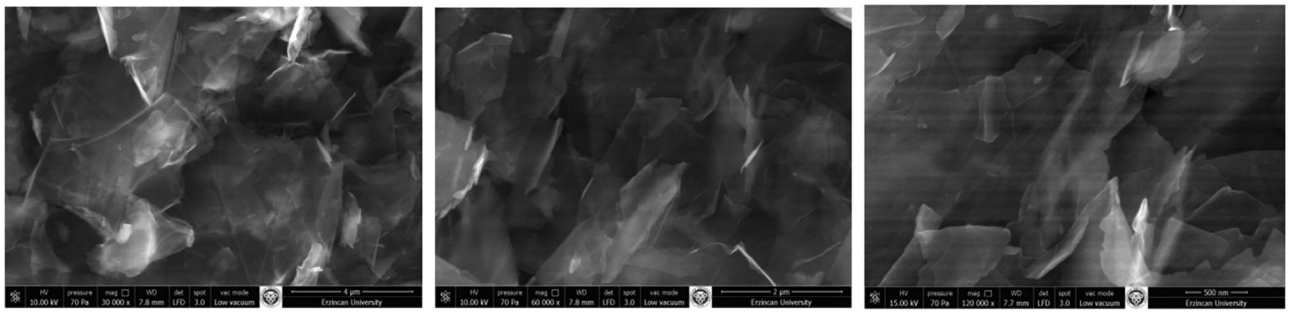


**Figure 1.** SEM images of GO at 4 µm, 2 µm, and 500 nm.


© 2020 Wiley-VCH GmbH

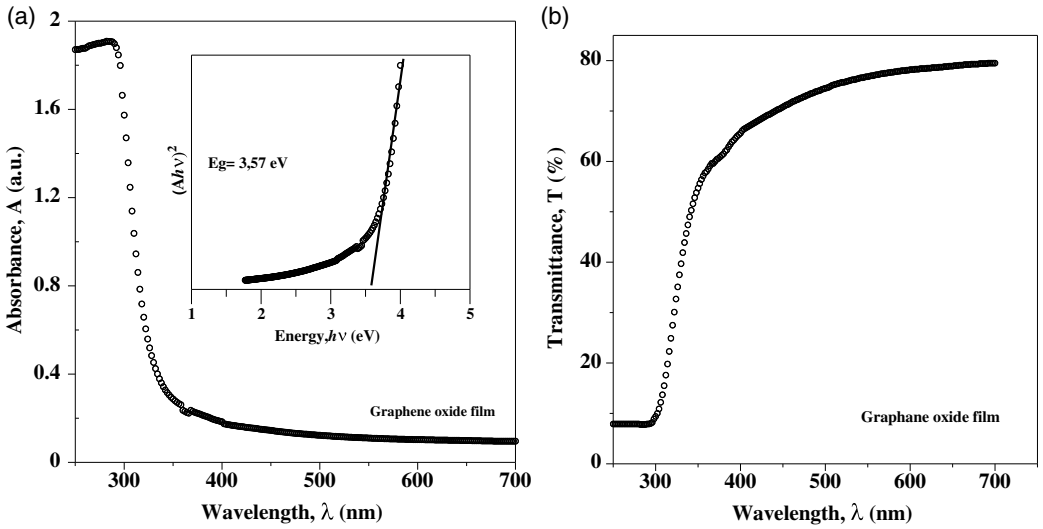



**Figure 3.** a,b) UV–vis characteristics and the transmittance spectra of the GO film.

bandgap and the bandgap of GO film was calculated as 3.57 eV. According to the data obtained, we can conclude that GO film is suitable for various applications such as solar cell applications.

The optical transmittance spectrum of the GO film is shown in Figure 3b. The optical transmittance values increased with the increasing wavelength and at wavelength of 700 nm reached a maximum value of 79.5%. As shown in **Figure 4**a,b, the absorbance and transmittance spectra of GO film are in consistent.

Figure 4a shows the forward and reverse bias semilogarithmic *I–V* characteristics of the Ti/GO/n-InP SB diode and Ti/n-InP reference diode. As shown in Figure 4a, the log *I–V* characteristics clearly show the effect of GO film at room temperature and the leakage current decreases significantly,[22] whereas the rectification performance is significantly improved. This decrease in leakage current value can be attributed to the increase in BH. As a result, the BH of the Ti/n-InP structure increased using the GO interface between the metal and the semiconductor. This indicates that the height of the barrier can be controlled by selecting the appropriate interface materials. This situation can be thought to be caused by the passivation of the n-InP semiconductor surface by the existing GO thin film. That is, the BH can be controlled and it is a very important

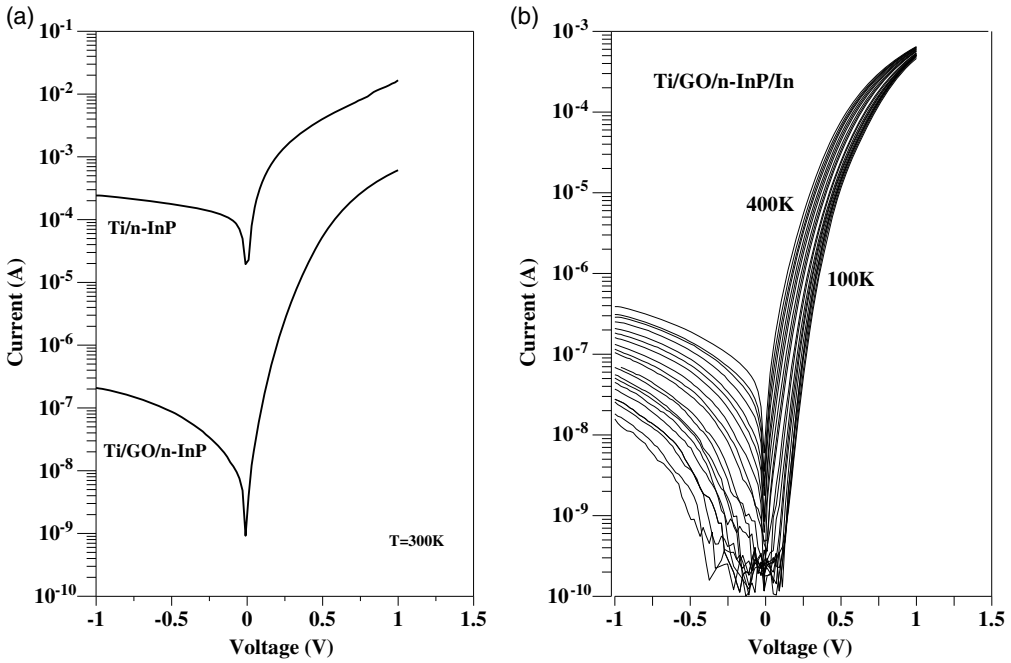



**Figure 4.** a) *I–V* characteristics for Ti/n-InP and Ti/GO/n-InP SBD at 300 K. b) *I–V–T* characteristics for Ti/GO/n-InP SBDs at various temperatures ranging from 400 to 100 K with a step of 20 K.


© 2020 Wiley-VCH GmbH

advantage for the MS junctions.[22] Figure 4a,b also shows the nonlinear region of the *I–V* curves at high forward bias due to the effect of the series resistance and the interface state density at the MS interface.

The Schottky diode parameters such as the ideality factor, BH, saturation current, and Richardson constant can be obtained from the classical method of analyzing the experimental *I–V* characteristics.[23,24] Particularly, the ideality factor and the BH are determined from the general equation of the current transport density which is usually described within the well-known thermionic emission (TE) theory given in Equation (1)[23]

$$I = I_0 \exp\left(\frac{qV}{nkT}\right)\left[1 - \exp\left(-\frac{qV}{kT}\right)\right] \tag{1}$$

where $I_0$ is the saturation current determined from extrapolating the linear region of the *I–V* plots and defined by

$$I_0 = AA^* T^2 \exp\left(-\frac{q\Phi_{b0}}{kT}\right) \tag{2}$$

where $n$ is the ideality factor which is dimensionless, $V$ is the applied bias voltage, $q$ is the electronic charge, $k$ is the Boltzmann constant ($k = 8.625 \times 10^{-5}$ eV K$^{-1}$), $T$ is the absolute temperature (Kelvin), $A$ is the rectifier contact area ($r = 0.25$ mm), $A^*$ is the effective Richardson constant (9.4 A cm$^{-2}$ K$^{-2}$ for n-type InP),[25,26] and $\Phi_{b0}$ is the experimental apparent BH. From Equation (1), it can be written as

$$\Phi_{b0} = \frac{kT}{q}\ln\left(\frac{AA^*T^2}{I_0}\right) \tag{3}$$

The ideality factor is a dimensionless parameter calculated from the slope of the linear region of the forward *I–V* characteristics, shows the bias dependent of the BH, and gives information about the ideality of the device.

$$n = \frac{q}{kT}\left(\frac{dV}{d\ln I}\right) \tag{4}$$

The temperature-dependent *I–V* characteristics of Ti/GO/n-InP SBDs were characterized to determine the transport properties of the diode. Figure 4b shows the experimental semilogarithmic forward and reverse bias *I–V* characteristics of Ti/GO/n-InP SBDs measured at temperatures from 100 to 400 K with 20 K steps. The experimental values of $\Phi_{b0}$ (apparent BH) and $n$ (ideality factor) have been determined from intercepts and slopes of the forward bias ln*I–V* plot at each temperature using the TE theory. The quality of a SBD is commonly determined by measuring the ideality factor ($n$). The ideality factor of the Ti/GO/n-InP SBD increased from 1.035 to 3.733, whereas the BH decreased from 0.980 to 0.263 eV (**Figure 5**a) when the temperature was decreased from 400 to 100 K in the presence of GO interlayer. The ideality factor value of the Ti/GO/n-InP SBD is higher than unity. The barrier inhomogeneity and the nonuniform distribution of the carriers in the interface may be attributed to the $n > 1$.[27] As $n$ values are bigger than unity, so it can be concluded that there is no pure TE in Ti/GO/n-InP SB device. This difference can be explained by the interface states or the barrier inhomogeneity in the interface of the Ti/GO/n-InP SBD.[28] At low temperatures, the decrease in the BH may be attributed to the lateral distribution of the SBH or the barrier inhomogeneities.[29,30] And the barrier inhomogeneities result in higher values of the ideality factor. In addition, the existence of the interfacial layers between the Ti/GO and GO/n-InP and several recombination centers or surface states near the surface of n-InP could be the reason of the ideality factor higher than unity ($n > 1$). Figure 5b shows the BH versus the ideality factor for the Ti/GO/n-InP SBD and also the dependence of the BH to the ideality factor is nonlinear. This nonlinearity is the result of the nonideality of the interface which is related to a bias-dependent barrier.[31]

It was reported that BH inhomogeneity has been explained by many current-transmission mechanisms.[25] However, it is clear that these explanations are not sufficient. The increase in the ideality factor at low temperatures cannot be explained just by the interface layer thickness or interface conditions. Especially at low temperatures, the Gaussian distribution function is the most usual and highly applicable method for clarifying the abnormal characteristics of the SBDs.[25] In the Gaussian distribution for a SBD with a BH $\bar{\Phi}_{b0}$ and its standard deviation $\sigma_s$, these parameters are linearly connected to the bias voltage and for such a distribution $\Phi_{ap}$ is the zero bias apparent BH and $n_{ap}$ is the

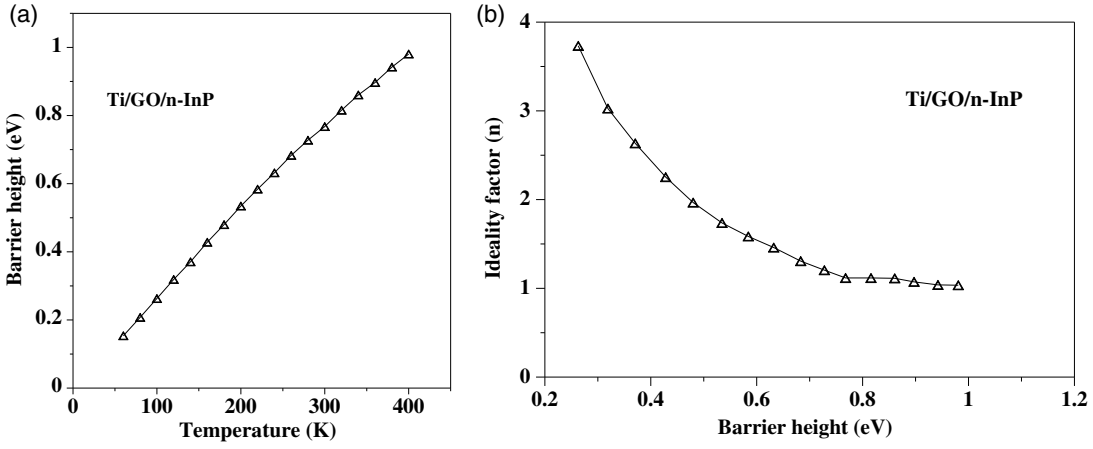



**Figure 5.** a) Temperature dependence of the BH. b) The BH versus the ideality factor for the Ti/GO/n-InP SBD.


© 2020 Wiley-VCH GmbH

apparent ideality factor. In ideal condition ($n = 1$), $\Phi_{ap}$ and $n_{ap}$ parameters are given by ref. [32]

$$\Phi_{ap} = \bar{\Phi}_{b0} - \frac{q\sigma_s^2}{2kT} \tag{5}$$

$$\left(\frac{1}{n_{ap}} - 1\right) = -\rho_2 + \frac{e\rho_3}{2kT} \tag{6}$$

By these expressions the dependence of $\sigma_s$ on temperature is usually small and negligible. According to Equation (6), the plot of $\Phi_b$ versus $1/2kT$ will be linear. Using the slope of this plot, the mean BH ($\bar{\Phi}_{b0}$) and standard deviation $\sigma_s$ can be found. The standard deviation gives information about the barrier homogeneity. That is, the standard deviation is a measure of the barrier homogeneity, and the lower of the standard deviation the higher homogeneous BH. However, the inhomogeneity and the potential fluctuations mostly affect the low temperature $I$–$V$ characteristics. In **Figure 6**, two linear regions were observed which indicates two Gaussian distribution region of 100–250 and 250–400 K temperature ranges. From the $\Phi_b$ versus $1/2kT$ plot, the mean BH and the standard deviation values were found to be $\bar{\Phi}_{b01} = 0.98$ eV, $\sigma_{s1} = -0.009$ eV (100–250 K) and $\bar{\Phi}_{b02} = 0.73$ eV, $\sigma_{s2} = -0.05$ eV (250–400 K) for the Ti/GO/n-InP Schottky diode, respectively. When compared with these mean BH values, the standard deviation values are not small and show the existence of Schottky barrier inhomogeneity in the Ti/GO/n-InP SBD. Barrier inhomogeneities may arise from the interfacial layer, interfacial layer thickness, the nonuniformity of interfacial charges, and the inhomogeneities in the composition. In such circumstances, the current through the contact may be greatly influenced by the presence of the BH inhomogeneity.[33] Likewise, the ideality factor shows two linear regions with temperature. These results show that the double Gaussian distribution of the height of the barrier occurred depending on the temperature.

Effective BH can be calculated with the help of conventional Richardson curves or activation energy curves. Accordingly, the current expression in Equation (2) can be edited and rewritten as follows

$$\ln\left(\frac{I_0}{T^2}\right) = \ln(AA^*) - \frac{e\Phi_b}{kT} \tag{7}$$

According to these equations, the zero bias BH and Richardson constant can be calculated from the temperature-dependent $\ln(I_0/T^2)$ versus $1/nkT$ graphs. However, the barrier is not homogeneous; the Richardson plot used to extract the Schottky BH deviates from linearity due the barrier inhomogeneity. In this case, it can be modified by combining Equation (2) and (5), which yields

$$\ln\left(\frac{I_0}{T^2}\right) - \left(\frac{q^2\sigma_s^2}{2k^2T^2}\right) = \ln(AA^*) - \frac{q\bar{\Phi}_{b0}}{kT} \tag{8}$$

We obtain modified activation energy of Richardson plot of **Figure 7**. As can be seen from the figures, these graphs have two separate linear regions. The first region is represented by the high-temperature region fit 1 (400–250 K) and the second region by the low-temperature region fit 2 (250–100 K). The slope of this graph gives directly the $\bar{\Phi}_{b0}$, and the mean BH of Ti/GO/n-InP SBD from here is $\bar{\Phi}_{b01} = 0.93$ and $\bar{\Phi}_{b02} = 0.69$ eV. These

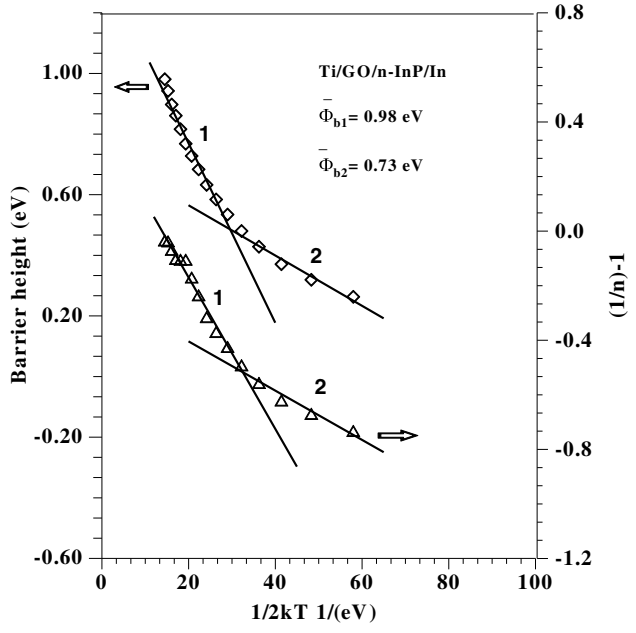



**Figure 6.** The BH and [(1/$n$)–1] versus $1/2kT$ of Ti/GO/n-InP SBD.

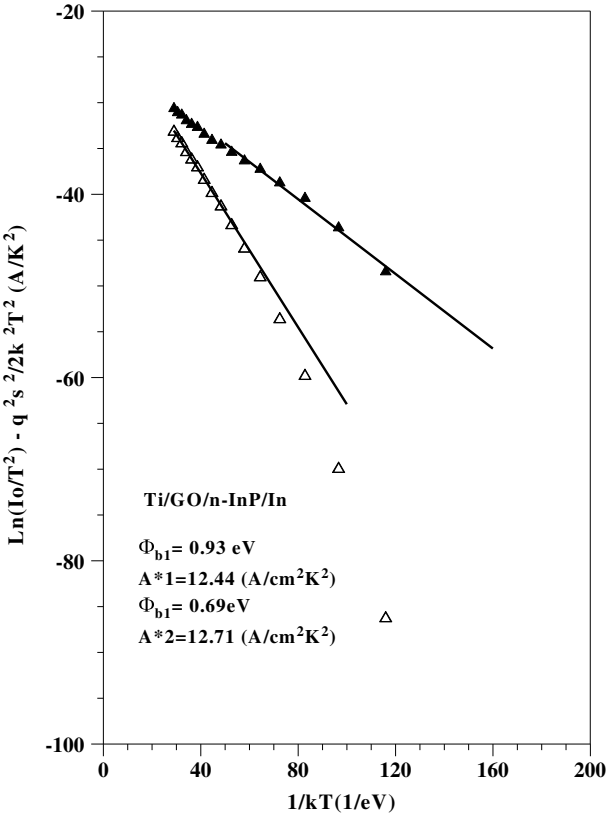



**Figure 7.** Modified Richardson plot of $\ln(I_0/T^2)$–$q^2\sigma^2/(2k^2T^2)$ versus $1/kT$ for Ti/GO/n-InP SBD.


© 2020 Wiley-VCH GmbH

mean BH values are in good agreement with those found from $\Phi_{b0}$ versus $1/2kT$ plot. The fact that the mean BH values calculated by two different methods are very close to each other confirms that the Ti/GO/n-InP SBDs fit the double Gaussian distribution of the barrier of the height. Again using the fit equation of this plot, the Richardson constant values for the Ti/GO/n-InP Schottky diodes are found to be $A^*_1 = 12.44$ and $A^*_2 = 12.71\ \mathrm{A\,cm^{-2}\,K^{-2}}$, respectively. These values seem to agree with the known Richardson constant, expressed in the literature as $9.4\ \mathrm{A\,cm^{-2}\,K^{-2}}$. The $A^*$ value obtained from the temperature-dependent $I$–$V$ plots may be affected by the lateral inhomogeneity of the barrier, and its discrepancy from the theoretical value may be related to the fact that the actual effective mass value is different from the theoretically calculated value.[34] It can be seen from these results that modified Richardson plots have showed two linear slopes of low- and high-temperature regions. The mean values of BHs and the Richardson constants for low- and high-temperature regions can be successfully expressed in terms of the TE mechanism with a double Gaussian distribution of Ti/GO/n-InP SBD.

Thus, the results obtained for Ti/GO/n-InP SB structures have been successfully explained by the Gaussian distribution of BHs based on the TE theory of temperature-dependent forward bias $I$–$V$ characteristics. Similar results have been observed in the literature in many studies.[25,35–37]

The capacitance of the space charge region in Schottky diodes gives important information on the formation of the metal/semiconductor interface. From the voltage dependence of the capacitance in the reverse bias, parameters such as BH, carrier concentration in the semiconductor, diffusion potential, and Fermi energy level of the rectifier contact can be determined.[38] The $C$–$V$ measurements for Ti/GO/n-InP SBD were performed at 1 MHz frequency, from −1 and 0 V and in the temperature range 100–400 K in steps of 20 K. **Figure 8**a shows the $C$–$V$ change (400–100 K) of the reverse bias at 1 MHz of the Ti/GO/n-InP SBD. As the reverse bias application voltage increases, the capacity rapidly decreases. Figure 8b shows the $1/C^2$–$V$ variation (400 and 100 K) obtained by using the reverse bias $C$–$V$ graphs of the Ti/GO/n-InP SBD. As can be seen from the graphs, while the application voltage decreases for the reverse bias region, $1/C^2$ decreases.

The $C$–$V$ measurements are evaluated by arranging Equation (9) for the diode capacitance as given below

$$C = A\left(\frac{\varepsilon_s \varepsilon_0 e N_d}{2}\right)^{\frac{1}{2}}\left(V_d - \frac{kT}{e}\right)^{\frac{1}{2}} \tag{9}$$

where $\varepsilon_s$ is the dielectric constant of the semiconductor ($\varepsilon_s = 12.4$ for InP), $\varepsilon_0 = 8.85 \times 10^{-14}\ \mathrm{F\,m^{-1}}$ is the dielectric constant of the cavity, $e$ is the electron charge, $V_d$ is the diffusion potential, $k = 8.625 \times 10^{-5}\ \mathrm{eV\,K^{-1}}$ is the Boltzman constant, $N_d$ is the ionized donor concentration, and $T$ is the temperature in Kelvin.

$$C^{-2} = \frac{2(V_d + V)}{\varepsilon_s \varepsilon_0 e A^2 N_d} \tag{10}$$

where $V$ is the applied voltage and $A$ is the area of the contact. The $C^{-2}$–$V$ plot has linear curves when obtained using Equation (10). With the convenient linear fit to $C^{-2}$–$V$ when the $C^{-2} = 0$, $V_d$ is equal to $V_d = -V$. Therefore, diffusion potential is obtained. Using these graphs, diffusion potentials at different temperatures were calculated for Ti/GO/n-InP SBD. The slope of the linear part of the $C^{-2}$–$V$ curves gives $d(C^{-2})/dV$ and after slope values were found, the $N_d$ carrier concentrations for each temperature were obtained by substituting in the expression (10). These values of $N_d$ varied from $7.5 \times 10^{23}\ \mathrm{cm^{-3}}$ and $9.4 \times 10^{22}\ \mathrm{cm^{-3}}$ for the Ti/GO/n-InP SBD (400–100 K). In addition, temperature-dependent changes in BH and carrier density values obtained from $C$–$V$ characteristics for the Ti/GO/n-InP SBD are shown in **Figure 9**a,b, respectively.

Fermi energy level values ($E_f$) of Ti/GO/n-InP Schottky diode determined from $C$–$V$ measurements were found to be 0.199–0.032 eV (400–100 K). In addition, BHs from the $C$–$V$ graph calculated by the difference between the conductivity band and the Fermi level and using the donor density were obtained from the slope. The BHs calculated from this correlation were between 1.328 eV (100 K) and 1.006 eV (400 K) for Ti/GO/n-InP SBD.

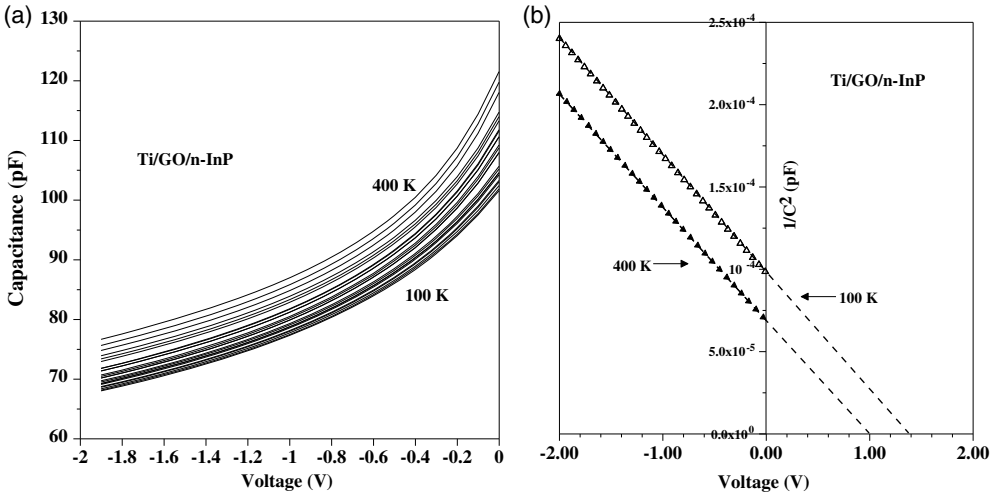



**Figure 8.** a) The plot of temperature-dependent reverse bias $C$–$V$ characteristics of Ti/GO/n-InP SBD ($f = 1$ MHz). b) The plot of temperature dependent $1/C^{-2}$ versus $V$ for Ti/GO/n-InP SBD (400 and 100 K).


© 2020 Wiley-VCH GmbH

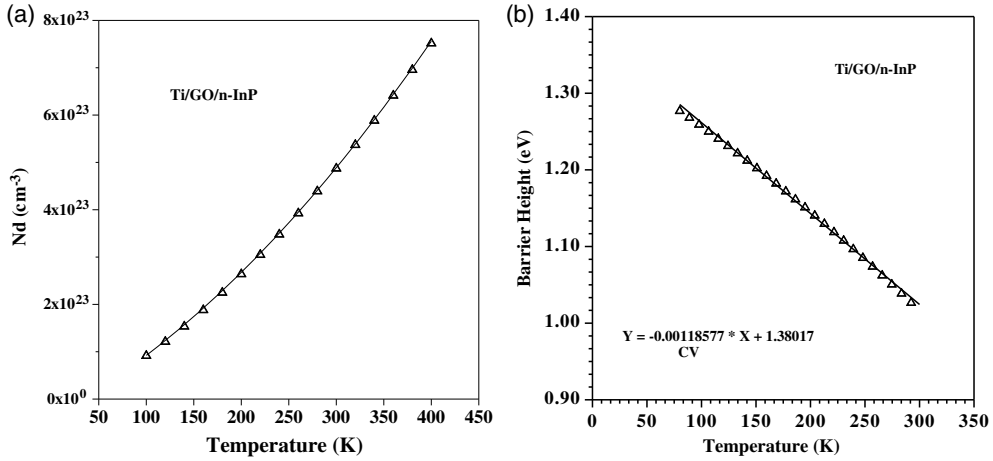



**Figure 9.** The temperature-dependent a) BH b) carrier density values of Ti/GO/n-InP SBD obtained from $C^2$–$V$ characteristics.

Figure 8b shows $\Phi_{C-V}$ values obtained from the reverse bias $C^{-2}$–$V$ characteristics depending on the sample temperature. The experimental $\Phi_{C-V}$–$T$ plot yields $\Phi_{C-V}$ $(T = 0) = 1.380$ eV and $\alpha = -1.186$ meV K$^{-1}$, where $\alpha$ is the temperature coefficient of the BH. Therefore, it was found that the BHs obtained from $C$–$V$ measurements were different at low and high temperatures. Such a behavior of this data shows an evidence of a double Gaussian distribution of BHs for the Ti/GO/n-InP SBD. In addition, as temperature increased, BH decreased, carrier densities increased, and Fermi energy increased. This situation is consistent with the literature. For sure, $I$–$V$ and $C$–$V$ measurement techniques were different from each other and it was seen that the ideality factors and BH s obtained from $I$–$V$ and $C$–$V$ measurement techniques were quite different. If the BHs are homogeneous and ideal, the measurements obtained from both measurement techniques should give the same results. Where homogeneity and ideality are not the norm, the measurements to be obtained from both measurement techniques will be different.[23]

An important case for both diode structures is that the BH ($\Phi_b$) values calculated from $I$–$V$ and $C$–$V$ measurements are different from each other as a function of temperature. The differences in the BH determined from $I$–$V$ and $C$–$V$ methods might be due to the inhomogeneity in the interface layer composition, nonuniformity of the interfacial layer thickness, and distribution of interface charges.[39]

As a result, in this study, the reverse bias leakage current of the Ti/GO/n-InP SB structure was significantly reduced with the GO thin film layer, which was enlarged by the chemical spraying method, and the BH value was increased from 0.224 to 0.768 eV at 300 K. Moreover, the temperature-dependent changes in the characteristic diode parameters were explained by the theory that the diode currents valid in both structures were provided by TE through a barrier with a double Gaussian distribution.

For $I$–$V$ and $C$–$V$ measurements especially at low temperatures, however, the BH decreases significantly while the ideality factor increases dramatically and image-force lowering, tunneling, recombination, and interfacial layers cannot account for this significant departure from unity of the ideality factor. Instead, an inhomogeneous barrier model can explain this behavior very well. An inhomogeneous barrier with a Gaussian distribution of BH s also results in a temperature dependence of the BH. Other parameters, such as carrier concentration, carrier mobility, series resistance, and ideality factor, may contribute to this temperature dependence as well.

## 3. Conclusion

In this study, Ti/GO/n-InP diode was obtained by growing GO film on n/InP semiconductor using spray pyrolysis method, which is an easy and economical method to apply. The morphological properties of the GO film and Ti/GO/n-InP SBD were carried out and the effects of GO interlayer on device performance were investigated in detail. The morphological and structural analysis of the GO film exhibited that GO film grown by spray pyrolysis was properly coated on the surface. The optical absorbance spectra showed that bandgap energy of the GO film was 3.57 eV. The optical transmittance values increased with the increasing wavelength and at wavelength of 700 nm reached a maximum value of 79.5%. In addition, the absorbance and transmittance spectra of GO film were in consistent. The Ti/GO/n-InP SBD showed almost 4 times more rectification behavior than the reference Ti/n-InP diode. The $I$–$V$ characteristics of this SBD in the temperature range of 100–400 K were analyzed using standard TE theory with assuming a Gaussian distribution of the BHs. The experimental $I$–$V$–$T$ values of BH and ideality factor were varied from 0.263 eV and 3.733 at 100 K to 0.980 eV and 1.035 at 400 K, respectively. The value of $\Phi_b$ increased and the $n$ decreased with increasing temperature. The $I$–$V$ characteristics of the Ti/GO/n-InP SBD over a wide temperature range showed two Gaussian distributions of BHs of 100–250 and 250–400 K temperature ranges due to the inhomogeneities present at the interface of the Ti/GO/n-InP SBD device. The mean BH values were found to be $\bar{\Phi}_{b01} = 0.98$ eV (100–250 K) and $\bar{\Phi}_{b02} = 0.73$ eV (250–400 K) from the $\Phi_b$–$1/2kT$ plot. From the modified Richardson plots based on a Gaussian distribution of BH, the mean BH of Ti/GO/n-InP SBD was $\bar{\Phi}_{b01} = 0.93$ (250–400 K) and $\bar{\Phi}_{b02} = 0.69$ eV (100–250 K) and $A^*$ was calculated to be 12.44 and 12.73 A cm$^{-2}$ K$^{-2}$, respectively. These BH values were


© 2020 Wiley-VCH GmbH

in good agreement with those found from $\Phi_b$ versus $1/2kT$ plot. And also $A^*$ values were in good agreement with the theoretical value for n-type InP semiconductor. Therefore, the temperature-dependent $I$–$V$ behavior of Ti/GO/n-InP SBD could be associated with the inhomogeneity in the BH. The BH s calculated from $C$–$V$–$T$ measurements were between 1.328 eV (100 K) and 1.006 eV (400 K) for Ti/GO/n-InP SBD. Therefore, it was found that the BHs obtained from $C$–$V$ measurements were different at low and high temperatures. Such a behavior of this data shows an evidence of a double Gaussian distribution of BHs for the Ti/GO/n-InP SBD. The $I$–$V$–$T$ and $C$–$V$–$T$ measurements conclude that carrier transport mechanism of Ti/GO/n-InP can be explained well by TE mechanism with a double Gaussian distribution of the SBHs and the Ti/GO/n-InP SBD has excellent electrical and optical properties for electronic and optoelectronic applications.

## 4. Experimental Section

Ti/GO/n-InP SBD was fabricated with n-InP (100) wafer as the substrate in this work. First, n-InP substrate was degreased in trichloroethylene, acetone, and methanol for 5 min each step by using ultrasonic agitation, and etched with hydrofluoric acid (48%) and $H_2O$ solution (1:10) within 1 min to remove the impurities and surfaces damages, and then quickly washed with deionized water. In (99.9%) metal was formed with thickness of 100 nm at a pressure about $10^{-6}$ mbar in NANOVAK NVTH-350 high vacuum system. To perform the ohmic contact, n-InP wafer was annealed at 350 °C for 1 min under a $N_2$ gas flow.

The synthesis of GO was carried out by easy and safe oxidation process of modified Hummers method from graphite.[3,40] To deposit GO film, 0.5 g GO powder was dispersed separately in 20 mL of ethylene glycol which have high dispersability with GO.[27,41] The GO film was deposited using spray pyrolysis technique which uses a liquid source for thin film coating onto preheated substrates with Holmarc's HD-TH-04 Spray Pyrolysis system.[42,43] The distance between the nozzle and the substrate was 20 cm. The GO film was deposited on the substrates with a thickness of 100 nm at 200 °C, whereas the deposition temperature was monitored with a digital multimeter. Compressed and filtered air was used as carrier gas. $1 \times 1$ mm$^2$ InP semiconductor and soda lime glass was used as the substrate for film depositing.

After film depositing, the GO films were dried at 100 °C for 20 min. Schottky junction was formed by using Ti (99.9%) metal deposited on the GO film as circular dots with 100 nm thickness (0.5 mm diameter) under $10^{-6}$ mbar by vacuum evaporation system. The surface morphology was characterized by Zeiss Supra 50 VP SEM. The structural properties of the GO film was performed with a Panalytical Empyrean X-ray diffractometer operated at 45 kV, 40 mA with Cu Kα radiation ($\lambda = 1.5406$ Å). The optical absorption and transmittance of GO film on glass substrate were performed using Perkin-Elmer Lambda 2S UV–vis spectrophotometer. The $I$–$V$ and $C$–$V$ measurements of the Ti/GO/n-InP SBD were obtained by using a Keithley 2400 and a 6514 Keithley electrometer and a HP model 4192 ALF impedance analyzer by using a closed-cycle He cryostat with 20 K temperature steps at 100–400 K temperature range under dark.

## Conflict of Interest

The author declares no conflict of interest.

## Keywords

$C$–$V$–$T$, graphene oxide, InP, $I$–$V$–$T$, Schottky diodes, spray pyrolysis method

Received: March 8, 2020
Revised: June 13, 2020
Published online: August 5, 2020

[1] L. Liao, H. Peng, Z. Liu, *J. Am. Chem. Soc.* **2014**, *136*, 12194.
[2] S. Park, R. S. Ruoff, *Nat. Nanotechnol.* **2009**, *4*, 217.
[3] W. S. Hummers, R. E. Offeman, *J. Am. Chem. Soc.* **1958**, *80*, 1339.
[4] C. Botas, P. Álvarez, P. Blanco, M. Granda, C. Blanco, R. Santamaría, L. J. Romasanta, R. Verdejo, M. A. López-Manchado, R. Menéndez, *Carbon* **2013**, *65*, 156.
[5] J. Song, X. Wang, C.-T. Chang, *J. Nanomater.* **2014**, *2014*, 1.
[6] A. Kocyigit, İ. Karteri, I. Orak, S. Uruş, M. Çaylar, *Phys. E* **2018**, *103*, 452.
[7] D. T. Phan, R. K. Gupta, G. S. Chung, A. A. Al-Ghamdi, O. A. Al-Hartomy, F. El-Tantawy, F. Yakuphanoglu, *Sol. Energy* **2012**, *86*, 2961.
[8] C. P. Liu, Y. Y. Hui, Z. H. Chen, J. G. Ren, Y. Zhou, L. Tang, Y. B. Tang, J. A. Zapien, S. P. Lau, *RSC Adv.* **2013**, *3*, 17918.
[9] M. Gülnahar, *Metall. Mater. Trans. A* **2015**, *46*, 3960.
[10] G. Niu, G. Capellini, F. Hatami, A. Di Bartolomeo, T. Niermann, E. H. Hussein, M. A. Schubert, H.-M. Krause, P. Zaumseil, O. Skibitzki, G. Lupina, W. T. Masselink, M. Lehmann, Y.-H. Xie, T. Schroeder, *ACS Appl. Mater. Interfaces* **2016**, *8*, 26948.
[11] S. B. Son, Y. Kim, B. Cho, C.-J. Choi, W.-K. Hong, *J. Alloys Compd.* **2018**, *757*, 221.
[12] O. Gullu, M. Cankaya, V. Rajagopal Reddy, *Indian J. Phys.* **2018**, *93*, 467.
[13] F. E. Cimilli, H. Efeoğlu, M. Sağlam, A. Türüt, *J. Mater. Sci.: Mater. Electron.* **2008**, *20*, 105.
[14] Y. Y. Kudryk, V. V. Shynkarenko, V. S. Slipokurov, R. I. Bigun, R. Y. Kudryk, *Semicond. Phys. Quantum Electron. Optoelectron.* **2014**, *259*, 210.
[15] Ç.Ş. Güçlü, A. F. Özdemir, A. Karabulut, A. Kökce, Ş. Altındal, *Mater. Sci. Semicond. Process.* **2019**, *89*, 26.
[16] P. R. S. Reddy, V. Janardhanam, I. Jyothi, S.-H. Yuk, V. R. Reddy, J.-C. Jeong, S.-N. Lee, C.-J. Choi, *J. Semicond. Technol. Sci.* **2016**, *16*, 664.
[17] Y. Munikrishna Reddy, R. Padmasuvarna, T. Lakshmi Narasappa, R. Padma, V. Rajagopal Reddy, *Indian J. Phys.* **2015**, *89*, 1161.
[18] Y. Munikrishna Reddy, R. Padmasuvarna, T. Lakshmi Narasappa, P. Sreehith, R. Padma, L. Dasaradha Rao, V. Rajagopal Reddy, *Superlattices Microstruct.* **2015**, *86*, 280.
[19] A. Bianco, H.-M. Cheng, T. Enoki, Y. Gogotsi, R. H. Hurt, N. Koratkar, T. Kyotani, M. Monthioux, C. R. Park, J. M. D. Tascon, J. Zhang, *Carbon* **2013**, *65*, 1.
[20] M. S. Eluyemi, M. A. Eleruja, A. V. Adedeji, B. Olofinjana, O. Fasakin, O. O. Akinwunmi, O. O. Ilori, A. T. Famojuro, S. A. Ayinde, E. O. B. Ajayi, *Graphene* **2016**, *05*, 143.
[21] N. Baraz, İ. Yücedağ, Y. Azizian-Kalandaragh, Ş. Altındal, *J. Mater. Sci.: Mater. Electron.* **2018**, *29*, 12735.
[22] A. Baltakesmez, A. Taşer, Z. Kudaş, B. Güzeldir, D. Ekinci, M. Sağlam, *J. Electron. Mater.* **2019**, *48*, 3169.
[23] E. H. Rhoderick, R. H. Williams, *Metal-Semiconductor Contacts*, Clarendon Press, Oxford University Press, Oxford [England], New York **1988**.
[24] A. Di Bartolomeo, *Phys. Rep.* **2016**, *606*, 1.
[25] F. E. C. Çatır, *Semicond. Sci. Technol.* **2020**, *35*, 035023.
[26] Y. M. Reddy, M. K. Nagaraj, S. S. Naik, V. R. Reddy, *J. Mod. Phys.* **2012**, *03*, 538.
[27] T. Çakıcı, *J. Mole. Struct.* **2020**, *1199*, 126945.
[28] A. Kocyigit, I. Orak, Z. Çaldıran, A. Turut, *J. Mater. Sci.: Mater. Electron.* **2017**, *28*, 17177.


© 2020 Wiley-VCH GmbH

[29] A. Di Bartolomeo, F. Giubileo, G. Luongo, L. Iemmo, N. Martucciello, G. Niu, M. Fraschke, O. Skibitzki, T. Schroeder, G. Lupina, *2D Mater.* **2016**, *4*, 015024.
[30] A. Di Bartolomeo, G. Luongo, F. Giubileo, N. Funicello, G. Niu, T. Schroeder, M. Lisker, G. Lupina, *2D Mater.* **2017**, *4*, 025075.
[31] R. F. Schmitsdorf, T. U. Kampen, W. Mönch, *J. Vac. Sci. Technol. B* **1997**, *15*, 1221.
[32] J. H. Werner, H. H. Güttler, *J. Appl. Phys.* **1991**, *69*, 1522.
[33] K. Ejderha, N. Yıldırım, A. Türüt, B. Abay, *Superlattices Microstruct.* **2010**, *47*, 241.
[34] Z. J. Horváth, *Solid-State Electron.* **1996**, *39*, 176.
[35] F. E. Cimilli, M. Sağlam, H. Efeoğlu, A. Türüt, *Phys. B* **2009**, *404*, 1558.
[36] G. Brezeanu, G. Pristavu, F. Draghici, M. Badila, R. Pascu, *J. Appl. Phys.* **2017**, *122*, 084501.
[37] H. Çetin, E. Ayyildiz, *Phys. B* **2010**, *405*, 559.
[38] R. H. Williams, G. Y. Robinson, C. W. Wilmsen, *Physics and Chemistry of III-V Compound Semiconductor Interface*, Plenum Press, New York **1985**.
[39] Y.P. Song, R.L. Van Meirhaeghe, W.H. Laflère, F. Cardon, *Solid-State Electron.* **1986**, *29*, 633.
[40] S. N. Alam, N. Sharma, L. Kumar, *Graphene* **2017**, *06*, 1.
[41] A. Kocyigit, I. Orak, Ş. Aydoğan, Z. Çaldıran, A. Turut, *J. Mater. Sci.: Mater. Electron.* **2017**, *28*, 5880.
[42] C. Guild, S. Biswas, Y. Meng, T. Jafari, A. M. Gaffney, S. L. Suib, *Catal. Today* **2014**, *238*, 87.
[43] D. Perednis, L. J. Gauckler, *J. Electroceram.* **2005**, *14*, 103.


© 2020 Wiley-VCH GmbH